Aalto University

Taghavi, Mehrdad; Ferrantelli, Andrea; Joronen, Tero

Multi-objective optimization of a plate heat exchanger thermal energy storage with phase change material

Research papers

Multi-objective optimization of a plate heat exchanger thermal energy storage with phase change material

Mehrdad Taghavi [a,*], Andrea Ferrantelli [b,c,d], Tero Joronen [a]

[a] *Department of Materials Science and Environmental Engineering, Tampere University, 33720, Tampere, Finland*
[b] *Department of Mechanical Engineering, Aalto University, 00076 Aalto, Finland*
[c] *Department of Civil Engineering, Aalto University, 00076 Aalto, Finland*
[d] *FinEst Centre for Smart Cities (Finest Centre), Tallinn University of Technology, Tallinn, Estonia*

ARTICLE INFO

ABSTRACT

The plate heat exchanger thermal energy storage system is recognized as a highly efficient form of latent heat thermal energy storage. However, existing studies show that the efficiency and performance of these thermal energy storage systems are significantly affected by the design variables, indicating the need of optimization studies. This investigation thus conducts a response surface modeling analysis based on validated computational fluid dynamics simulations. Four design variables of the system are identified, and through response surface modeling the values of five responses such as average power and average effectiveness are predicted within the defined range of the design variables. A multi-objective optimization model then determines the optimal configuration of design variables for all responses, based on the response surface modeling and validated simulations. The results indicate that the optimal design has 21.4 % higher effectiveness than the normal design. The system also achieves maximum performance by employing 5 mm of the phase change material section thickness considering all the efficiency parameters. Moreover, charging the system over 10 °C above the PCM's melting temperature significantly decreases efficiency while providing minimal enhancement to power.

$$\overline{\varepsilon}(t) = \frac{\int_0^t \left(\frac{T_e(t') - T_i}{T_0 - T_i} \right) dt'}{t}, \tag{1}$$

1. Introduction

Thermal energy storage (TES) plays a crucial role in shaping the future of sustainable energy systems, as it enhances the energy efficiency and cost-effectiveness of traditional energy systems by effectively capturing, storing, and distributing thermal energy [1]. Among all the variants of TESs [2], the systems with phase change materials (PCMs) are more feasible to be used in compact energy systems, since using PCMs significantly decreases the volume of the TESs and increases their thermal capacity [3]. In these systems, the PCM changes between solid and liquid phases, absorbing heat from the heat transfer fluid (HTF) as it liquefies (charging process) and releasing the stored heat as it solidifies (discharging process). Despite the advantages of PCM-based TESs, the stored thermal energy in the systems cannot be released efficiently due to the low thermal conductivity of the conventional PCMs, causing prompt changes in the outlet temperature of HTF, T_e [4]. According to Eq. (1) which calculates the average effectiveness of TESs, $\overline{\varepsilon}$, as

using HTF inlet temperature, T_i, and the initial temperature of the TES at the beginning of the charging/discharging process, T_0, this immediate T_e change decreases the effectiveness [5].

In addition to effectiveness, the average thermal power, $\overline{P}$, and restored heat from the TES, Q, which are respectively obtained as

$$\overline{P}(t) = \frac{\int_0^t \dot{m}_h C_{P(h)} (T_e(t') - T_i) dt'}{t}, \tag{2}$$

$$Q(t) = \int_0^t \dot{m}_h C_{P(h)} (T_e(t') - T_i) dt' \tag{3}$$

are also considered for evaluating the performance of a TES [5]. In these equations, $\dot{m}_h$ and $C_{P(h)}$ represent the mass flow rate and specific heat capacity of HTF. Similar to $\overline{\varepsilon}$, the average thermal power and the restored heat also decrease in response to the drop in T_e according to Eq.

Nomenclature

RSM	response surface modeling
MOOP	multi-objective optimization problems
CFD	computational fluid dynamics
d	sections' thickness (mm)
$\dot{m}$	flow rate (kg/s)
P	thermal power (kJ/s)
$\vec{g}$	gravitational acceleration
$\vec{s}$	source term
$\vec{u}$	velocity vector
Amushy	mushy zone constant
Cp	specific heat capacity (kJ/kg.K)
f	liquid fraction of PCM
H	total enthalpy (kJ/kg)
h	sensible enthalpy (kJ/kg)
k	thermal conductivity (W/m.K)
L	latent heat of PCM (kJ/kg)
M	mass (kg)
Q	stored/released energy (kJ)
T	temperature (K)

t	time (s)
t2°C	the duration required for a 2 °C temperature drop time in the heat transfer fluid outlet temperature
0	initial condition
p	process
HTF	Heat transfer fluid
PCM	phase change material
ref	reference
m	melting process
s	solidification process

Greek symbols

ε	effectiveness
μ	viscosity (kg/m.s)
$\bar{\varepsilon}$	average effectiveness
ρ	density (kg/m^3)

Subscripts

e	HTF outlet condition
h	heat transfer fluid
i	HTF inlet condition

(2). In addition, the low heat transfer rate between PCM and HTF increases the charging process time of the PCM-based TESs, which restricts the use of these TESs in fast-response systems.

To summarize, PCM-based TESs need a feasible solution to tackle the low thermal conductivity of PCMs and reach higher efficiency and more reliable performance.

Enhancing the heat transfer rate between PCM and HTF by increasing the heat transfer surface between these two fluids in the TESs is a practical solution to defer the T_e change during charging or discharging processes. To achieve this, plate-type thermal energy storage systems (PTESs) have been presented as they can provide a massive heat transfer surface within a compact system. Stathopoulos et al. [6] introduced a plate-type TES consisting of multiple aluminum containers filled with PCM, designed for a ventilation system. The airflow in the system passes over these containers absorbing/releasing heat from/to the PCM. These TESs have significantly higher efficiency and improved performance than the other types of PCM-based TESs. However, the high risk of deformation in the containers or capsules due to the significant volume change of PCMs during the processes [7] hinders the containers from being fully filled with PCM, and consequently, the TES cannot reach the maximum thermal capacity.

To overcome the deformation problem, roll-bonded PTESs have been proposed by Saeed et al. [8], in which the PCM is stored in a vessel and HTF flows through roll-bonded plates to exchange heat with the PCM. This design significantly increases the effectiveness of the system and removes the risk of deformation during the charging and discharging processes. A comparison between this plate-type TES and a conventional storage system shows up to 83.1 % enhancement in the system's efficiency which proves the impact of this high heat transfer surface on the system's performance [8]. In addition, Lin et al. [9] presented a plate-type TES using pillow plates and the results of this study show a significant improvement in heat transfer rate between the HTF and PCM compared to the traditional energy storages.

Despite the significant improvements in the efficiency of the TESs using the plate design, the need for costly changes to increase/decrease the thermal capacity of the system raises concerns about implementing such TESs in large-scale energy systems. In addition, these PTESs still experience a significant rate of temperature change during the initial stages of melting or solidifying, limiting their ability to maintain a constant temperature [7]. Moreover, these studies show that the T_e drop is still significant in these systems.

Taking an efficient and thermal capacity flexible PTES into account, Gürel [11] has studied the phase change of paraffin in a plate heat exchanger (PHE) using a computational fluid dynamics (CFD) model. The results show that the melting time in this PTES drops by 75 % compared to a cylindrical TES. However, as the studied model is two-dimensional and the HTF flow is assumed to be homogeneous and fully developed, the results are not reliable for a realistic geometry of this type of TESs [12,13].

Taghavi et al. [14] presented a highly efficient and cost-effective plate heat exchanger thermal energy storage system (PHETES) which is depicted in Fig. 1. This TES has a similar structure to a PHE in which heat is transferred through the metal plates from the high-temperature fluid to the low-temperature fluid.

However, unlike PHEs, only one fluid (water in this study) flows in the PHETES, and the second fluid (PCM) is stored within the system. The results of this study show a 75 % enhancement in energy storage capacity compared to the roll-bonded PTES. In addition, the PHETES can discharge the stored heat with a more stable T_e than a conventional PTES. Moreover, using metal plates instead of roll-bonded plates and vessels provides more flexibility in the thermal capacity of the system and decreases manufacturing costs.

Since the heat transfer rate between the PCM and HTF is low at the upper side of the PHETES (due to low HTF velocity in this area), the PCM sections are loaded up to the HTF connections, and the upper part (the gap shown in Fig. 1.b) will remain empty to balance the volume change of PCM during the melting process. Hence, the system can balance the PCM expansion without any significant effect on the system's efficiency.

Adding to the promising improvement in the efficiency and performance of the plate-type TESs with the presented PHETES, the authors of [14] observed that the efficiency of these systems is determined by their design and operating conditions. This was confirmed by other studies on TESs showing the effect of HTF flow rate [9], plate spacing [8,15], HTF inlet temperature [6,16], and thermal conductivity of the utilized PCM [4] on the performance and efficiency of PTESs. An optimization study is thus required to reach the optimal design for the presented PHETES, by considering all these important parameters for the targeted energy system.

Since the performance and efficiency of TESs are evaluated with several parameters, hereafter called "efficiency parameters", improving
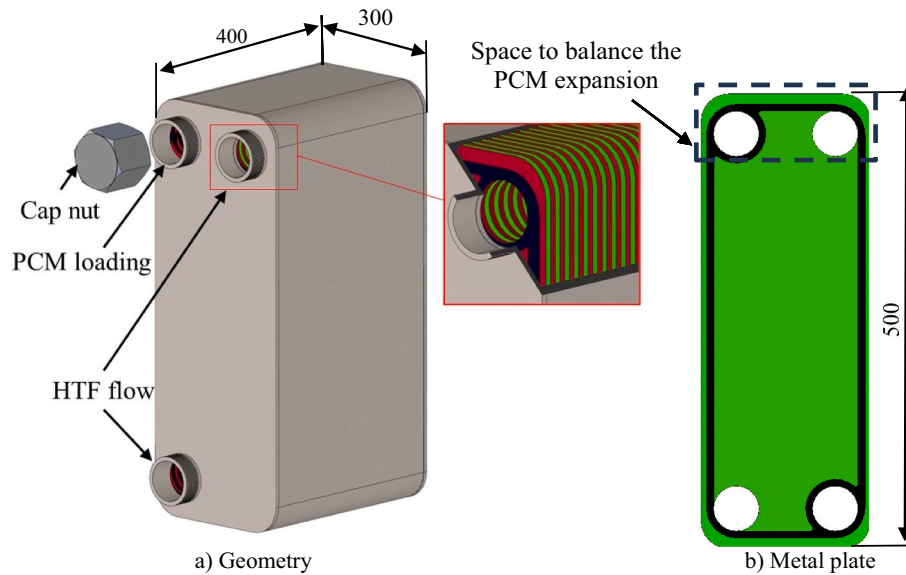
Fig. 1. Schematic of the proposed PHETES by Taghavi et al. [14].

one of them might negatively affect the others or the total efficiency of the system; in a study of a plate-type TES that was used in a solar air conditioning system, it was observed that improving the efficiency of the system increases the charging time of the TES [17]. A similar work on a molten salt TES illustrates that although raising the inlet T_i significantly improves the charging time, a more non-uniform phase change rate will be observed at a higher T_i [18].

Another study on a plate-type TES shows that increasing T_i significantly accelerates the phase change process in TESs, while it raises the energy consumption of the system [19]. Unlike the HTF temperature though, changing plate inclination has no additional cost or energy use of the system. Hence, although optimizing the plate inclination has a lower effect on the TES' performance, this optimization is more feasible to enhance the performance of the TES, rather than increasing T_i.

Therefore, the geometrical parameters of a TES should be carefully investigated in the design process even though they have less effect on the efficiency parameters than the operational parameters. In addition, the effect of design/operational variables on all efficiency parameters which are important for the defined energy system should be considered carefully.

Experimental design, which is an analytical method to study different combinations of design factors in a product or system to identify the optimal design [20], is used to study the design variables and optimize them in an industrial product such as TESs [21]. However, the traditional experimental design methods are mostly complex, time-consuming, and challenging to reach the desired objectives [22].

To overcome these problems, Taguchi presented a model to study all effective design variables with a minimum number of experiments [23]. Another approach to experimental design analysis is the response surface methodology (RSM), which is widely used in such studies [24]. According to the literature, RSM requires more experiments than the Taguchi method [25], yet it is an effective method for conducting an in-depth study of the effects of design variables on efficiency factors [26]. A combination of these two methods is also utilized in [26], to optimize the melting performance in a storage tank by using the Taguchi design to present the optimum fin distribution, the number of fins, and the fins material. Then an RSM model based on the Taguchi designs was used to study the effect of fin length, width, and rotation angle.

A similar investigation has been carried out on a TES with a flip mechanism to study the effect of inner tube eccentricity, fin deflection angle, and fin width on melting performance. The Taguchi method is utilized to analyze the individual contributions of each parameter to the

melting performance, and the interactions of design variables are determined by using RSM [27]. Although the Taguchi method shows promising results in predicting the response values, there is some common agreement that the RSM technique is more accurate [28].

The thermodynamic properties of the utilized PCM in a TES can be involved in an optimization study in addition to geometric parameters and operating conditions. Enhancing the thermal conductivity of the PCM by using copper nanoparticles was considered as a solution to improve the heat transfer rate in a TES, together with increasing the heat transfer surface by using fins and raising natural convection with a rotational mechanism [29]. However, the results show that the effect of nanoparticles is not as significant as the improvement in the geometry of the TES. In addition, the optimization decreases the melting time by 74 % compared to the original design, while the thermal capacity drops by 4.1 %.

Such studies prove the importance of optimization studies on TESs as an optimal design that can significantly enhance the system's performance. Due to the significance of the optimization and the lack of such studies on the proposed PHETES [14], the current research focuses on a comprehensive optimization study on this specific TES. The results show that the optimal design has significantly higher efficiency than the normal design, if the HTF and PCM sections' thicknesses, as well as the temperatures T_i and T_0, are considered as the design variables.

2. Methodology

The discharge process of the PHETES with an upward HTF (water in this study) flow serves as the case study to identify the optimal design for delivering heat to the energy system (Fig. 5 in [14]).

In addition to HTF flow direction and type of process, this study assumed as constant design parameters both the overall size of the PHETES (as depicted in Fig. 1) and the thermophysical properties of the utilized PCM (as referenced in Table 2, ref. [14]). In addition, since the study at hand aims at optimizing the presented PHETES to operate with a domestic heat pump as an energy system for a residential apartment, $\dot{m}_h$ equals 0.15 kg/s, in order to meet the operating conditions of this energy system [30,31].

Two main design variables T_i and T_0, considered as operational design parameters, optimize the PHETES in this study. The thickness of the HTF section, d_{HTF}, and that of the PCM section, d_{PCM}, are instead considered as geometrical design variables.

Since T_e in the TESs decreases over time during the discharge process

[4] and the aim of presenting the PHETES is providing a stable T_e to the heating system, the duration for which the T_e drop is <2 °C, $t_{2°C}$, is considered as the main response parameter in this study. The restored heat from the PHETES after this time is the next response we considered, as obtained from Eq. (3) by using $t_{2°C}$ as the upper bound of the integral. In addition to the stability in delivering the restored heat, the overall process time, t_p, which is the required time to freeze all the PCM within the PHETES, is also considered as a parameter to compare the different designs of the PHETES. The other response parameters are $\bar{\varepsilon}$ and $\bar{P}$, which are obtained from Eqs. (1) and (2) by considering t_p as the upper bound of the integral. All of the above design parameters and responses are summarized in Table 1.

The utilized methodologies in this research are CFD models, to simulate the phase change process in the PHETES with the defined design variables, RSM models to predict the responses' values over the defined design variables, and finally MOOP to propose the optimal design.

The utilized methodologies in this research are CFD models, to simulate the phase change process in the PHETES with the defined design variables, RSM models to predict the responses' values over the defined design variables, and finally, Multi-Objective Optimization Problems (MOOP) to propose the optimal design.

2.1. CFD model

To avoid time-consuming and costly experiments to analyze the effect of each design variable on the efficiency parameters, this study employed a transient model to simulate the heat transfer between PCM and HTF as well as the PCM phase change. The equations that are utilized in this model are continuity, momentum, and energy, which are presented as,

$$\frac{\partial \rho}{\partial t} + \nabla.(\rho \vec{u}) = 0,$$ (4)

$$\frac{\partial \rho \vec{u}}{\partial t} + \nabla.(\rho \vec{u} \vec{u}) = -\nabla P + \mu(\nabla^2 \vec{u}) + \rho \vec{g} + S,$$ (5)

$$\frac{\partial (\rho H)}{\partial t} + \nabla.(\rho \vec{u} H) = \nabla.\left(\frac{k}{C_p}\nabla H\right)S_h,$$ (6)

respectively [32]. In these equations, ρ, H, $\vec{u}$, P, $\vec{g}$, and S_h represent density, enthalpy, velocity vector, pressure, gravitational acceleration, and energy source term. S also denotes momentum reference term and is given by

$$S = \frac{(1-f)^2}{f^3}A_{mushy}\vec{u},$$ (7)

where A_{mushy} is the mushy zone constant [33]. The values of f are also calculated as,

$$f = \begin{cases} 0, & if\ T < T_{solidus}, \\ 1, & if\ T > T_{liquidus}, \\ \dfrac{T - T_{solidus}}{T_{liquidus} - T_{solidus}}, & if\ T_{solidus} < T < T_{liquidus}. \end{cases}$$ (8)

Because phase change does not occur in the HTF, the enthalpy in Eq. (6) is solely a function of temperature for the HTF, while this parameter is affected by both temperature and phase change (latent heat) in the PCM. As a result, the HTF enthalpy, H_{HTF}, in the energy equation is calculated as

$$H_{HTF} = h_{ref} + \int_{T_{ref}}^{T} C_P\, dT',$$ (9)

and the PCM enthalpy, H_{PCM}, is obtained as

$$H_{PCM} = f.L + h_{ref} + \int_{T_{ref}}^{T} C_P\, dT',$$ (10)

where L is the total amount of latent heat for the PCM; the reference state is defined as the initial condition of the TES before starting the processes [11].

As depicted in Fig. 1, the PHETES comprises multiple interconnected HTF and PCM sections arranged in a linear configuration. Since simulating the complete geometry requires a substantial number of grids and considerable computational resources, the PHETES' geometry is simplified to Fig. 2.a which includes one PCM section surrounded by two HTF sections. However, since the model is symmetric, half of the geometry is considered in the CFD model for more simplification (Fig. 2.b).

Since Taghavi et al. experimentally validated the presented CFD model of the PHETES and carried out the mesh independence study on the model (Section 4 in [14]), the exact same CFD model of the PHETES is used in this study.

According to Section 5.1 in [14], the highest relative error is 6.26 % indicating a good agreement between the experiments and simulation results across various geometries and operating conditions within the defined range. Additionally, Fig. 8 in [14] reveals that the model's accuracy remains largely consistent across different HTF flow rates as changing the flow rate increases the relative error only up to 2.9 %. A similar conclusion can be drawn by comparing Fig. 9.a and b with Fig. 9. c and d in [14] regarding the impact of HTF inlet temperature on the

Table 1
Design variables, constant parameters, and responses.

Parameter type	Parameter name	Label	Unit	Physical range	Coded	Coded range
Design variable	HTF thickness	d_{HTF}	mm	[5, 20]	A	[−1,1]
	PCM thickness	d_{PCM}	mm	[5, 20]	B	[−1, 1]
	Initial T	T_0	K	[343, 360]	C	[−1, 1]
	HTF inlet T	T_i	K	[296, 310]	D	[−1, 1]
Constant parameters	HTF flow rate	$\dot{m}_h$	Kg/s	0.15	–	–
	PHETES size	–	mm	500 * 400 * 300	–	–
	Metal plate thickness	–	mm	1	–	–
PCM's thermophysical properties	Melting temperature	T_m	K	337	–	–
	Solidification temperature	T_s	K	332.5	–	–
	Latent heat	L	kJ/kg	270	–	–
	Specific heat capacity	Cp	kJ/kg·K	2–29.62	–	–
	Thermal conductivity	k	W/m·K	0.22–0.34	–	–
Response	Average power	$\bar{P}$	kW			
	Restored heat	Q	kJ			
	Average effectiveness	$\bar{\varepsilon}$	–			
	Time to 2 °C drop	$t_{2°C}$	s			
	Process time	t_P	s			
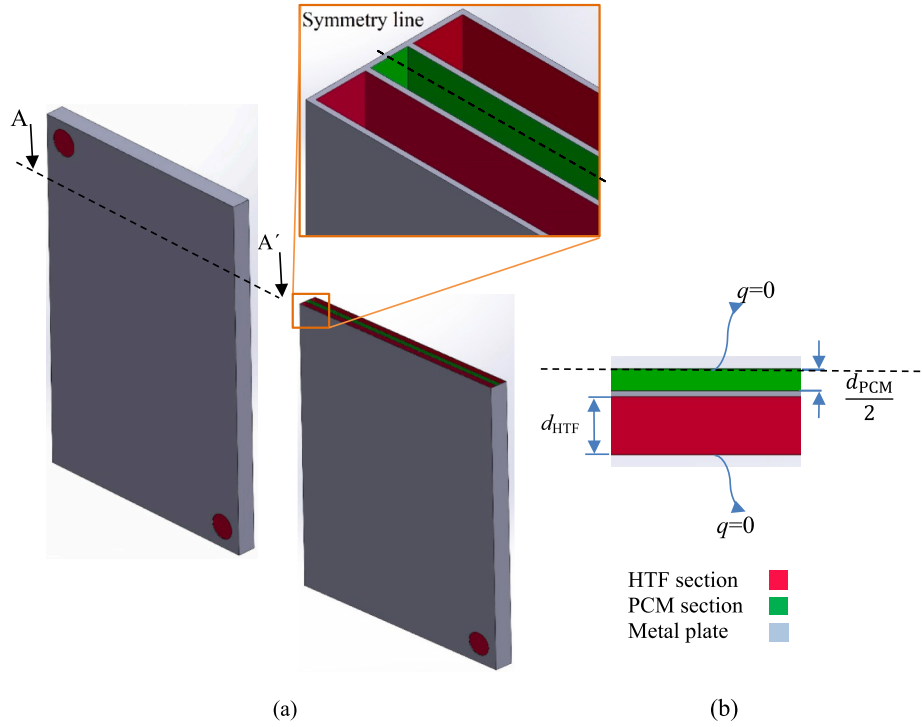
Fig. 2. The simplified geometry of the PHETES including two HTF sections and one PCM section (a), top view of the utilized geometry in the CFD model (b).

model's accuracy. Comparing Figs. 8 and 10 in [14] shows that changing the HTF and PCM section thicknesses affects the relative error by 3.3 % which shows the model is reliable for different geometries. Moreover, the results of the mesh independence study (Fig. 7 in [14]) show that the grid size barely affects the model's results.

In summary, since the proposed model is reliable with different geometries and operating conditions and there is no significant deviation between the experiments and the simulations' results, the proposed model is used in this optimization study.

Computing the Reynolds number using the specified HTF flow rate, HTF thickness, and width indicates that the maximum Reynolds number is 400. This value suggests laminar flow for the HTF, which aligns with the proposed model for PHETES (Section 5 in [14]).

As a result of the mesh, operating conditions, and geometry sensitivity studies, as well as the flow regime study, this model is reliable for this optimization study, delivering the required data for the RSM investigation.

2.2. Response surface model

The response surface methodology is adopted for studying the relationship between a set of parameters, which we shall call "design variables" and correspond to the PHETES design characteristics, and a set of "response variables", which reflect the performance of the energy storage system.

In general, a polynomial regression model is generated by the RSM according to the design variables' assigned range; this will express each of the responses y as a polynomial function of the n design variables x_i. For the case at hand, we shall use a most customary second-order model,

$$y = a_0 + \sum_{i=1}^{n} a_i x_i + \sum_{i=1}^{n} a_{ii} x_i^2 + \sum_{i,j \neq i}^{n} a_{ij} x_i x_j + \sigma, \tag{11}$$

with a_0, a_i, a_{ii}, a_{ij} as the coefficients of the constant, linear or first order (FO), pure quadratic (PQ), and two-way interaction (TWI) terms, respectively. σ is a statistical error that is naturally embedded within the model by construction.

Specifically, we shall be looking for five distinct second-order regression formulas, to quantify how five PHETES performance parameters (response variables, or responses) are influenced by each of the device's design variables. Both of these parameter sets, including the ranges of design variables, are given in Table 1.

In this investigation, we have used the "RSM" package for R [34], to which we remand for further details. Although RSM is quite intricated from the viewpoint of statistical methodology, the procedure is quite straightforward: once the design variables and the k responses have been defined, experimental or simulated values of the k responses are fitted by the RSM engine, which returns k regression formulas. It is then possible to study how the responses' values change in function of a single design variable, or of specific combinations of them.

2.2.1. Experimental design: combining Box-Behnken design with training and testing sets

It is quite well known that one of the main challenges in RSM practice is finding a set of experimental observations that would be optimal. This means that the experiments (here, simulations) should determine the set of response values in such a way that the prediction power of the regression formulas Eq. (11) is high, at the same time minimizing the number of experiments of simulations, which are time and resource consuming. In this paper, we adopt the Box-Behnken design [35] with 4 factors corresponding to the $n = 4$ design variables in Eq. (11), which was successfully used in a similar context by Gao et al. [36].

The BBD (Box-Behnken Design) constructs a hypercube within the configuration space of the design variables, in this case, a 4-dimensional space, where each so-called "natural" variable x_i with a physical range of values mapped to a coded variable $X_i \in [-1, 1]$ in this new configuration space. Following common practice, these coded variables are labeled from A to D. The transformation formula is very simple and is listed below,

$$X_i = \left(x_1 - \frac{x_{1,max} + x_{1,min}}{2} \right) \frac{2}{x_{1,max} - x_{1,min}}, \tag{12}$$

where e.g., $X_i \equiv A$ is the first design variable, the HTF thickness $d_{HTF} \equiv x_1$.

With 4 variables and a 3-point design, we have obtained 27 simulations; the alternative central-composite response design (CCRD) used by e.g. Liu et al. [37], would have required 31 simulations. As running physical experiments or computer simulations is often time- and resources-consuming, the BBD method is sometimes chosen over CCRD for this very reason; however, the first 18 simulations from the first two BBD blocks returned some overfitting for the RSM with low predictive capabilities. The stationary point of the fitted surface was outside of the experimental region for some response variables. In such cases, one either adds the third and final BBD block (9 additional simulations) or employs a variety of techniques, such as the steepest ascent, which allows circumventing this problem by rescaling the coded variables [34].

Since this would anyway have required additional simulation runs and/or changed our chosen PHETES design variables' ranges that are listed in Table 1, we extended the BBD design by including off-set points (i.e., not −1, 0 or +1). The total set of 49 simulations then provided substantial testing for the RSM regression formulas that had been calculated.

Using a testing set besides a training dataset was indeed another purpose of our investigation. A major objective of BBD or CCRD designs is limiting the number of experiments; in data science, one typically uses a subset of data for training the model, with the remaining data as testing ground.

We have accordingly identified three different models, each of them containing the BBD design with 75 % training data and 25 % testing data, a share that is quite customary. By listing the simulation runs sequentially, Model 1 features the first 37 simulations, Model 2 the last 37, and Model 3 the 37 in the middle. 12 runs, allocated differently according to each model, were then used for testing. Each model's performance is investigated in Appendix A; several optimization options for PHETES design with enhanced flexibility were thus available, and for each response variable we selected either Model 2 or Model 3, according to the best performance.

For consistency with previous investigations, we have also calculated as a performance metric a parameter called R^2-prediction [37],

$$R^2_{pred} = 1 - \frac{PRESS}{SS_T}, \tag{13}$$

whose reliability against the testing datasets for the three models was checked. In the above equation, the total sum of squared differences between individual data points (y_i) and the mean of the response variable (y) is defined as

$$SS_T = \sum_i (y_i - y)^2. \tag{14}$$

PRESS, for "predictive RSS", is a version of the residual sum of squares (RSS) that sums up the squares of all the resulting prediction errors [39]. We recall that the RSS is defined as

$$RSS = \sum_i (\widehat{y}_i - y)^2, \tag{15}$$

where $\widehat{y}_i$ is the i-th predicted data point.

While the RSS describes how well a linear model fits the fitted data, the PRESS indicates how well the model will predict *new data*. This is intended to replace relying on training and testing sets, thus reducing the number of simulations in concordance with a BBD or CCRD design. As it is shown in Appendix A, at least in our case the PRESS (thus, R^2_{pred}) revealed not to be fully equivalent to using testing data, rather generating some tension.

2.3. Multiobjective optimization model

Multiobjective optimization is used in many different research fields, from scientific and technological design to economic investigations. The

main purpose is finding an ideal trade-off among two or more "objects" since they can seldom be maximized or minimized in the same configuration of the system that is considered. For example, we could look at balancing between maximizing return and minimizing risk.

In this paper, we look for a PHETES design that, given the five design variables identified in the previous section, would return the best possible compromise between maximal power, average effectiveness, and $t_{2°C}$, while minimizing the process time.

Multi-Objective Optimization Problems (MOOP) are quite difficult to solve and require sophisticated statistical insight. Here we have chosen a subclass of algorithms known as the Multi-Objective Evolutionary Algorithm, an extension of the so-called Genetic Algorithms for MOOP called Non-dominated Sorting Genetic Algorithm II (NSGA-II) [40], which shares elitism and crowded comparison. "Elitism" means that at each iteration, the best solutions of the previous iteration are kept unchanged, which significantly improves the convergence speed. It is also computationally simpler, as it uses a fast non-dominated sorting algorithm.

Ultimately looking for the optimal fitness value of one response variable, from a population of randomly selected chromosomes, or solutions, the algorithm computes the fitness values or the objective function values from each solution; two of these solutions will be chosen as parent solutions, then they will be crossed to create new solutions, called child solutions. At the end of the iteration, based on the fitness values a new population will be chosen, either from the parent solutions or the initial population and the child solutions. The algorithm will continue iterating until the stopping criterion (typically, the number of iterations) is fulfilled.

In MOOP, NSGA-II works a bit differently. At the end of each iteration, the new population for the next iteration is chosen with a non-dominated sorting method: the solutions are divided into several "Pareto fronts" and only those from the best front are chosen. Pareto optimality is the state where resources are allocated as efficiently as possible, in a way that improving one response will not worsen the others [41].

Moreover, the crowding distance (i.e., the Manhattan distance of two neighboring solutions for two objectives) of each solution is also computed for controlling the diversity of solutions. Those with the largest crowing distance are selected. As an exercise for testing the chosen NSGA-II algorithm and comparing the results with the literature, we have applied it to the regression formulas obtained by Liu et al. [37], Eqs. (18) to (20) in that paper.

By using the same desirability function methodology as in Gao et al. [36], for $t_{charging}$, Q, and η they respectively obtained 138.9 min, 140.7 MJ, and 65.9 %, corresponding to 4, 22, 672.8 K, 4 m/s, and 463 K for fins and tubes number, fluid inlet temperature, fluid velocity in the main channel, and initial temperature.

With NSGA-II, we instead obtained 137.78 min, 141.28 MJ, and 66.46 %, with parameters as follows: 6, 23, 673 K, 4 m/s, and 463 K. It therefore seems that NSGA-II could slightly improve those previous findings.

3. Results and discussions

This section articulates as follows: first, the results of the RSM model, which predicts the responses' values over the defined design variables, are presented. The optimal designs proposed by the MOOP model are then illustrated in Section 3.2.

3.1. Response surface model results

The present study uses a testing dataset comprising 49 CFD simulations; some statistical parameters are given in Table 2. By splitting the above set into 75 % training and 25 % testing simulation runs, we identified three distinct RSM models according to how the splitting was executed. For each of the 5 responses, we chose the best performing

Table 2
Statistical parameters of the full simulated dataset (49 observations).

	$\overline{P}$ [kW]	Q [kJ]	$\overline{\varepsilon}$ [−]	$t_{2°C}$ [s]	t_P [s]
Average	11.55	4979.66	0.394	169.54	1013.06
SD	4.49	1365.58	0.148	47.68	460.37
Ave/SD	2.57	3.65	2.67	3.56	2.2
Maximum	3.03	7998.83	0.65	249.20	2600
Minimum	23.85	1298.84	0.15	61.63	540

model according to testing set and prediction metrics, as illustrated in Appendix A. Model 3 was used for average power, restored heat, and average effectiveness, while $t_{2°C}$ and t_p were better predicted with Model 2 (Table 3).

As a first check for the goodness of fit for each of the five responses, the chosen regression model provides the R^2 values listed in Table 4, for both testing and training sets (the adjusted R^2 are slightly lower, but only at the third digit, thus they are omitted). R^2 and R^2_{pred} are both satisfactory and, as a metric of comparison, they are in line with the values reported in [36,37].

Diagnostic plots of predicted-vs-actual for average effectiveness are given in Fig. 3.a for the training data ($R^2 = 0.9896$) and in Fig. 3.b for testing data ($R^2 = 0.986$). Testing data diagnostic plots for Average power and process Time are given in Fig. 4 and Fig. 5, respectively. Diagnostics of the RSM regression models are addressed in the next section. The effect of design parameters on the efficiency parameters can be observed in Fig. 6. According to Fig. 6.a, the temperature drop in T_e happens faster with large PCM thicknesses while PHETES with a thick HTF section provides a more stable T_e as it can store greater volume of high-temperature HTF in the charging process. Then, discharging the stored fluid takes more time than a thin HTF section which gives more stability in T_e. In addition, this figure shows that increasing the PCM thickness accelerates the temperature drop. This is because thick PCM reduces the number of HTF sections in the system, resulting in a lower amount of high-temperature HTF that can be stored in the system. The PHETES power profile over the thickness of the sections is presented next. Comparing Fig. 6.a and b shows that changing the thickness has almost the same effect on power and temperature drop. According to Fig. 6.a, increasing the thickness of the HTF section delays the outlet temperature drop in the PHETES. Combining this outcome with Eq. (2), it can be concluded that increasing this thickness leads to raising the PHETES power as seen Fig. 6.b.

Unlike the PCM thickness, the thickness of the HTF section barely affects the average power, since Fig. 6 shows that increasing this thickness improves this efficiency parameter only slightly. Due to the low thermal conductivity of PCM and substitution of the high-temperature HTF with a colder fluid, the difference between T_i and T_e at the end of the discharging process is minimal, leading to a significant reduction in power. Since fully discharging the PHETES requires running the system for a long time while it has low power, the average power remains nearly constant for all scenarios regardless of the section's thickness.

However, Fig. 6.c shows that the PHETES performance is significantly affected by the thickness of the HTF section when the system is

working with stable T_e. According to this figure, a thick HTF section enhances the heat delivery of the system due to deferring the T_e drop.

T_0 and T_i are other design variables whose effect on the average effectiveness is presented in Fig. 6.d. This figure shows that $\overline{\varepsilon}$ reaches its maximum value when T_0 and T_i are at their minimum in the defined range. According to Eq. (3), the average effectiveness drops by increasing the PHETES initial temperature and the HTF inlet temperature. Fig. 6.e shows that T_i also has the same effect on process time, meaning that increasing T_i raises the process time: this change drops the temperature difference between the HTF and PCM, resulting in a poor heat transfer rate between these two fluids, according to Eq. (2). Such a low heat transfer rate increases the process time. However, as depicted in this figure, this design parameter has no significant effect on t_P when T_i reaches its low values in the range. Furthermore, a PHETES with a high T_0 requires more time to cool down the melted PCM to the solidification temperature and to start the freezing process, causing a long process time. On the other hand, analyzing Fig. 6.e, we can infer that a low T_0 also raises the process time due to the low temperature difference with the inlet HTF.

3.1.1. Regression formulas and ANOVA diagnostics

The output of the RSM methodology highlighted in Section 2.2 consists of four second-order regression formulas, each of them expressing a response variable in function of combinations of the four PHETES design variables, namely

$$y = A + B + C + D + AB + AC + AD + BC + BD + CD + A^2 + B^2 + C^2 + D^2 \tag{16}$$

The coefficients for each term in the regression formulas are listed in Table 4.

We recall that in the above, A = HTF thickness, B = PCM thickness, C = initial temperature, and D = HTF inlet temperature.

Regarding the regression model's diagnostics, the autocorrelation test provided excellent results for all the training datasets that are addressed in Appendix A. All five responses are within the boundaries in the autocorrelation function (ACF) plot, and residuals are well controlled (namely, the previous value has no impact on the next value). As no autocorrelation has been detected, systematic errors can be excluded.

Next, the ANOVA (or Analysis of Variance) illustrates if the model is valid and which combinations of those four PHETES design variables are most impactful on the five response variables. This is mostly determined by two parameters, the *F*-value, and the *p*-value. Specifically, the *F*-value is the variance of the group means (Mean Square Between) over the mean of the within-group-variances (Mean Squared Error). Such test statistic is therefore an indication of the variance of the model. Then, given an *F*-value, the *p*-value is the probability of getting a result at least as extreme as the one that was observed if the null hypothesis is true.

We shall reject the null hypothesis (namely, we can conclude that the model is significative) when the *p*-value is smaller than our chosen α-level, of the significance level. This usually corresponds to 5 %, or 0.05. Among the various combinations of PHETES design variables that are addressed by the RSM model, only those with *p*-value < 0.05 will be significant for the according response variable.

The ANOVA table for the chosen RSM models, all responses, is given in Table 5, where FO=First Order, TWI = Two-Way Interaction, and PQ = Pure Quadratic (see Section 2.2 for their definition).

Each of the three groups above therefore shows significance. Specifically, the combinations B, C, D, BD, and B^2 have significant effects on Power; A, B, C, D, E, A^2, B^2, C^2 on Restored heat; B, C, D, B^2 and C^2 are significant for average Effectiveness; A, B, C, AB, AC, AD, A^2, B^2, C^2 for $t_{2°C}$; B, D, BD, B^2 and D^2 for process Time.

Table 3
R^2 and R^2_{pred} values for the five response variables, RSM model with 4 design variables, 37 training (75 %), and 12 testing data (25 %).

	Training set	Testing set	R^2_{pred}
Average power [kW]	0.9866	0.9885	0.962
Effectiveness [−]	0.9896	0.986	0.974
2°K T drop time [s]	0.9924	0.9634	0.961
Time [s]	0.9828	0.9739	0.929
Restored heat [kJ]	0.9252	0.9565	0.752

Table 4

Regression formulas coefficients for the five responses, according to Eq. (16).

	Restored heat	Average power	Effectiveness	T drop time	Process time
(Intercept)	5159.862	9.608739	0.310517	165.7956	1052.391
A	1425.647	0.724549	0.026141	54.66348	28.00193
B	−1372.08	−6.3799	−0.21456	−54.0577	642.7175
C	306.379	1.157608	−0.02056	−17.0902	17.7118
D	−761.787	−2.13894	−0.02184	−0.615	151.2519
AB	203.2855	0.47472	0.020051	24.29791	11.12913
AC	−38.0746	0.435962	0.00989	−10.5583	−27.9252
AD	13.94874	0.293869	0.007588	−7.29192	0.947421
BC	−34.8235	−1.17597	−0.00054	1.202283	22.94741
BD	151.3882	0.945995	0.006569	−3.34783	152.9627
CD	−9.72036	0.101674	0.000981	0.618995	6.833863
A^2	−1282.07	−0.9273	−0.02945	−24.5291	−56.9185
B^2	601.648	2.61961	0.088713	17.76234	172.6255
C^2	−518.71	0.155417	0.012232	−12.8173	9.35918
D^2	−22.0342	−0.34538	−0.01109	−0.85039	63.76622

(a)

(b)
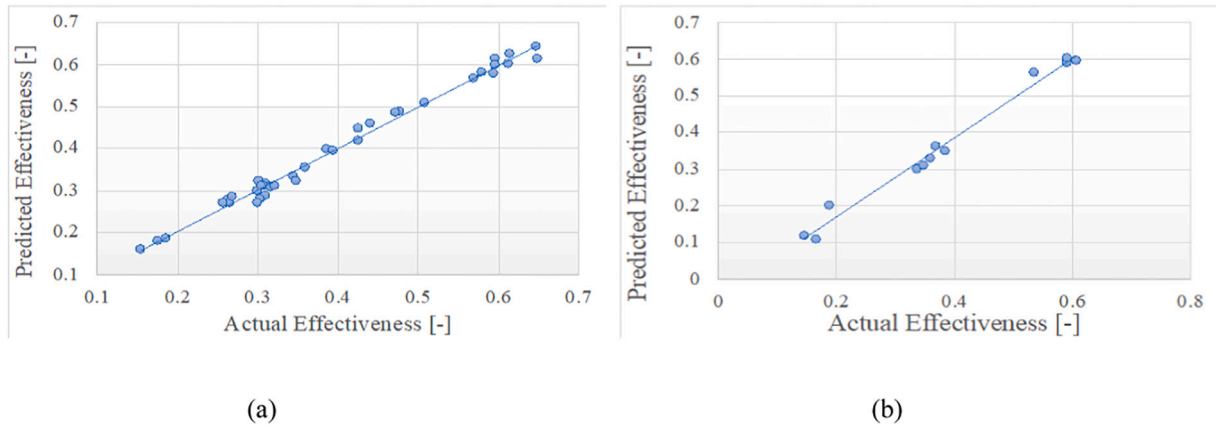
Fig. 3. Predicted (y-axis) vs actual (x-axis) data for Effectiveness, training data $R^2 = 0.9896$ (a), testing data $R^2 = 0.9896$ (b).
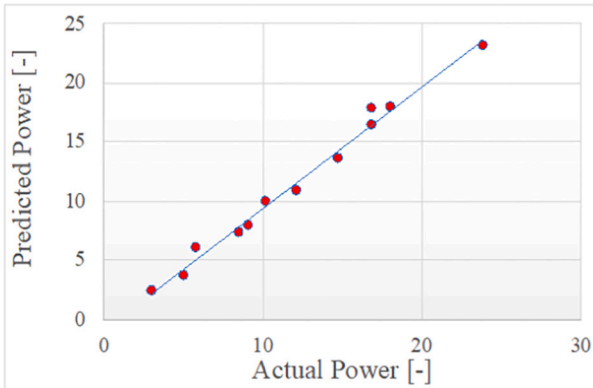
Fig. 4. Predicted (y-axis) vs actual (x-axis) data for Average power, testing data. $R^2 = 0.989$.
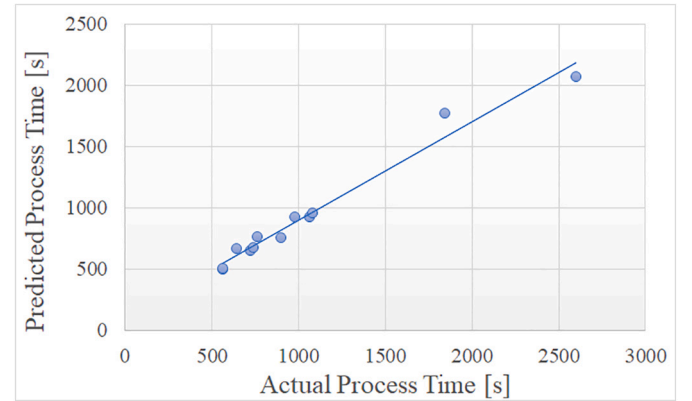
Fig. 5. Predicted (y-axis) vs actual (x-axis) data for process Time, testing data. $R^2 = 0.974$.

3.2. Multi objective optimization results

Table 6 displays the MOOP results when optimizing either average Effectiveness or average Power, for a population of 200 solutions and 1000 generations for the NSGA-II algorithm, including the values of responses as well as those of the according design variables.

It is immediately evident that the PHETES requires the minimum PCM thickness to achieve optimal performance. According to the conduction heat transfer equation, $Q = -kA\,\Delta T/d$, where A, ΔT, and d, are respectively the heat transfer area, the temperature difference between the surfaces, and the thickness of the part, low values of k can be compensated by decreasing the thickness. As a result, the PHETES can reach higher performance using lower PCM thickness instead of increasing the PCM's thermal conductivity.

Unlike the PCM thickness, the thickness of the HTF section varies based on the desired efficiency parameter. Additionally, according to this table, the thickness of HTF should not fall below 10 mm as there is no optimal efficiency parameter below this value. In addition, Table 6 shows that the PHETES reaches the optimal performance considering all the responses with the minimum value of T_i due to heat transfer enhancement according to Eq. (2). In other words, a low value of T_i

(a)   (b)

(c)   (d)

(e)
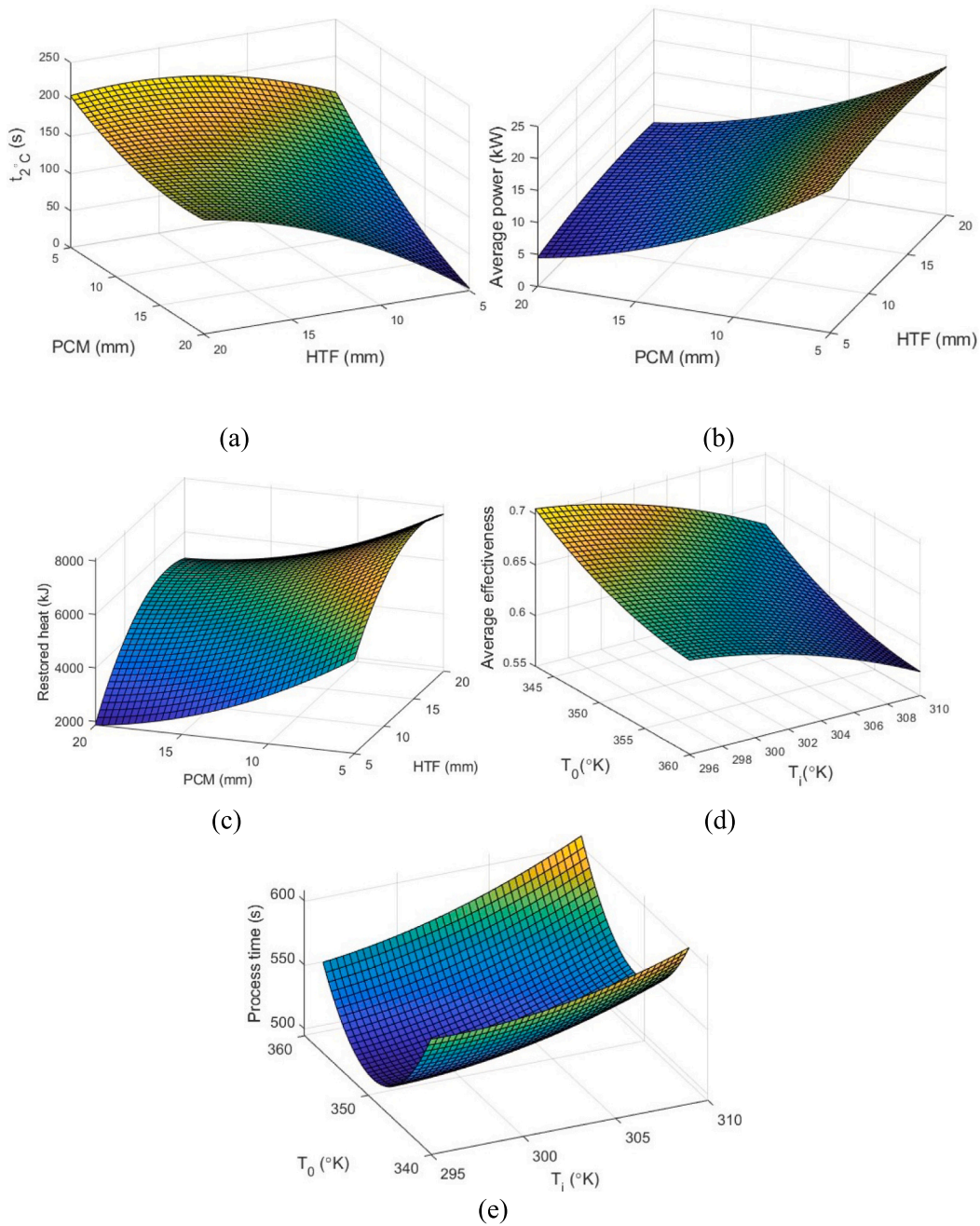
Fig. 6. Surface plots for $t_{2°C}$, average power, and restored heat as functions of PCM and HTF thicknesses (a), (b), and (c), average effectiveness and process time, based on T_0 and T_i (d), and (e).

Table 5
ANOVA results for the 5 responses with 4 design variables.

		Power [kW]	Restored heat [kJ]	Effectiveness [−]	$t_{2°C}$ [s]	t_p [s]
FO	*F*-value	378.3896	65.0906	493.8793	629.388	300.1049
	p-Value	<2.2e-16	7.506e-13	<2.2e-16	<2.2e-16	<2.2e-16
TWI	*F*-value	6.5081	2.5078	9.0627	29.123	4.5142
	p-Value	0.0004664	0.0487380	4.790e-05	2.148e-09	0.003983
PQ	*F*-value	17.9127	8.4728	18.1885	46.030	6.7511
	p-Value	1.132e-06	0.0001829	9.984e-07	2.217e-10	0.001054

increases the heat transfer between the HTF and PCM which can improve the effectiveness, power, temperature drop time, and process time.

Analyzing with Table 6 the effect of T_0 on the efficiency parameters for optimal designs reveals that a high temperature charging can slightly improve the thermal power, while it has negative effects on other parameters. Moreover, the PHETES is aimed to be used with heat pumps in which a high operating temperature reduces the efficiency [42]. As a

Table 6
MOOP results with NSGA-II (population = 200, 1000 generations).

	Min t_p [s]	Max $\bar{\varepsilon}$ [−]	Max $\bar{P}$ [kW]	Max Q [kJ]	Max $t_{2°C}$ [s]
$\bar{P}$ [kW]	16.66	19.33	**23.77**	21.9	17.9
Q [kJ]	6208	6866.5	8047.1	**8363.9**	7142.8
$\bar{\varepsilon}$ [−]	0.615	**0.665**	0.623	0.62	0.625
$t_{2°C}$ [s]	233	230	207	237	**264**
t_p [s]	**495**	636	659	657	640
HTF [mm]	10.5	11.1	14.1	16.0	19.9
PCM [mm]	5	5	5	5	5
T_0 [K]	347.5	343	360	354.2	343
T_i [K]	304.7	296	296	296	296
HTF volume fraction [−]	0.63	0.64	0.705	0.72	0.746
PCM volume fraction [−]	0.3	0.29	0.25	0.225	0.187
Plates volume fraction [−]	0.07	0.07	0.045	0.055	0.067

The bold identifies the optimisation target (Max or Min value) for the response variable the specific column refers to.
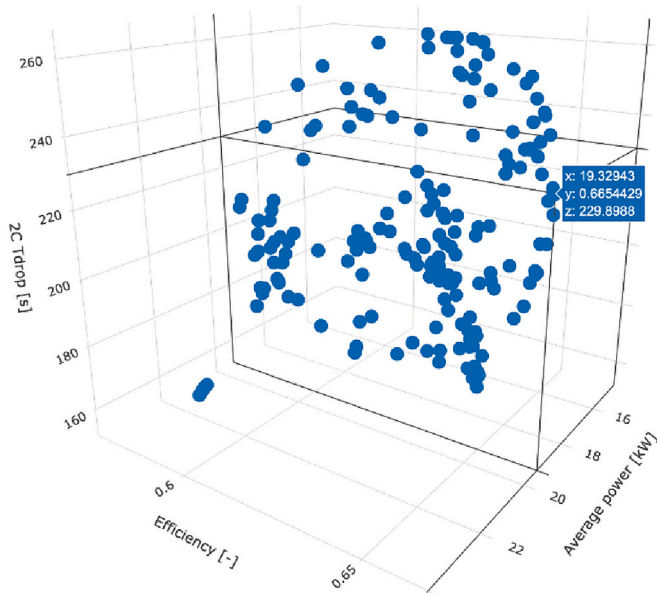
Fig. 7. MOOP results: 3D plot for optimal Efficiency as in Table 4, 1st Pareto front.

result, exceeding 10 °C from the melting temperature decreases the overall efficiency of the system.

Fig. 7 reports a 3D plot showing the distribution of solutions that belong to the first Pareto front, also called "dominant solutions", in the 4-dimensional space of configurations of the responses (the process time holds as 658.6 and Restored heat as 6866.104 kJ). The first Pareto front is the set of optimal solutions in the space of objective functions; these solutions are non-dominated to each other, but they are superior to all the other solutions [43].

As a side note, we conclude this section with a brief test and comparison for the NSGA-II algorithm. As an additional exercise, we have applied it to the regression formulas obtained by Liu et al. [37], Eqs. (18) to (20). Using the same desirability function methodology as in Gao et al. [36], for $t_{charging}$, Q, and η they respectively obtained 138.9 min, 140.7 MJ, and 65.9 %, corresponding to 4, 22, 672,8 K, 4 m/s, and 463 K for the number of fins, of tubes, fluid inlet T, fluid velocity in the main channel, and initial T.

With NSGA-II, we obtained 137.78 min, 141.28 MJ, and 66.46 %, with parameters as follows: 6, 23, 673 K, 4 m/s, and 463 K, which seems to be a good result.

4. Conclusions

This study carried out an optimization study of a plate heat exchanger thermal energy storage (PHETES) [14], by using a combination of response surface methodology models, computational fluid dynamics simulations, and multi-Objective Optimization Problems to identify the optimal design considering the efficiency parameters of the system. Average effectiveness, average power over the discharging process, the duration required for a 2 °C temperature drop time in the heat transfer fluid outlet temperature, and process time were tested against four main design variables: the thickness of the sections, the initial temperature of the system, and the inlet temperature of the heat transfer fluid. The main gains of our investigation are as follows:

The PHETES with a 5 mm phase change material section exhibits the highest performance for all the efficiency parameters.

A combination of 5 mm and 20 mm thickness for phase change material and heat transfer fluid, respectively, optimized all the responses except the process time.

Since the PHETES power drastically drops at the end of the discharging process, running the system to be fully discharged is not efficient for the energy system.

Considering the PHETES and heat pump efficiency, the system should not be charged by >10 °C above the PCM melting temperature.

This study shows the importance of RSM and multi-objective optimization for enhancing the efficiency and performance of a PHETES working with a heat pump. However, the benefit of the optimal design on the entire system is not clear. Therefore, further studies are required to evaluate both the energy savings and performance improvements of a heat pump with the PHETES against the additional costs incurred by the system. Additionally, the RSM analysis, although satisfactory, has unveiled some possibility for improvement that should be investigated as well.

CRediT authorship contribution statement

Mehrdad Taghavi: Writing – review & editing, Writing – original draft, Validation, Resources, Methodology, Data curation. **Andrea Ferrantelli:** Writing – review & editing, Writing – original draft, Validation, Methodology, Data curation. **Tero Joronen:** Writing – review & editing, Supervision, Resources.

Declaration of competing interest

The authors declare that they have no known competing financial interests or personal relationships that could have appeared to influence the work reported in this paper.

Data availability

Data will be made available on request.

Acknowledgments

The authors are grateful for support by the Paavo V. Suominen Fund

Appendix A. Comparison of training datasets for RSM

This section briefly discusses different experimental designs ("training sets" henceforth) for the RSM. By using only a BBD model, an ANOVA analysis showed that the stationary point of the fitted surface was far from the experimental region; further simulations were thus needed, due to a rescaling of the parameters' ranges following e.g., the steepest-ascent method.

As remarked in Section 2.2.1, we wanted to keep this experimental design, also aiming at testing datasets the regression formulas with new data outside the training set, since the parameters for transformation and optimization are in-sample. Such additional statistics then allowed exploring different empirical models, showing the importance of *testing* datasets.

The total number of simulations was 49, which we used to identify three models with a customary 75 % data for training (37 simulations) and 25 % for testing (12 simulations). Referring to the simulation runs as a sequence, Model 1 takes the first 37 simulations, Model 2 the last 37, and Model 3 has the central 37 simulations, in other words runs #1 to #6 and #44 to #49. This is similar to cross-validation (CV) in standard data analysis (we could actually say that we have performed a 3-fold CV).

Table A.1
Comparison of three different training sets for RSM.

	Model 1	Model 2	Model 3
Average power			
R^2 training	0.9909	0.9904	0.9866
R^2 testing	0.9106	0.985	0.9885
R^2_{pred}	0.975	0.977	0.962
Restored heat			
R^2 training	0.9808	0.92	0.9252
R^2 testing	0.649	0.9473	0.9565
R^2_{pred}	0.936	0.66	0.752
Effectiveness			
R^2 training	0.9918	0.9908	0.9896
R^2 testing	0.9522	0.9885	0.986
R^2_{pred}	0.978	0.978	0.974
T drop time			
R^2 training	0.9972	0.9924	0.9943
R^2 testing	0.7629	0.9634	0.959
R^2_{pred}	0.992	0.961	0.98
Process time			
R^2 training	0.9909	0.9828	0.9803
R^2 testing	0.7515	0.9739	0.9641
R^2_{pred}	0.947	0.929	0.918

Table A.1 illustrates a comparison of the three models by using the R^2 parameter for the three different training sets (R^2_{pred} was defined in Section 2.2.1). One can immediately notice how *testing* results clearly favor Model 3 for Average power, Restored heat and Average effectiveness, while $t_{2°C}$ and process time are better predicted with Model 2. Interestingly, at least for this dataset using R^2_{pred} as the sole performance parameter would have been deceiving for both T drop and process times, as R^2_{pred} was maximal for Model 1, while this model has the worst predictability for both.

As we deem the performance on the *testing* dataset to be the most reliable for predictions, the RSM analysis that is illustrated in Section 3.1 combines two of the above models: Model 2 for $t_{2°C}$ and process time, and Model 3 for Average power, Restored heat and Average effectiveness.

Of course, here we are not questioning common practice; it might be however worth exploring what is found in Table A.1 on a larger testing dataset, for example to see what happens if the three models are tested on the exact same testing dataset (by construction of 3-fold CV, this was not possible here). Exploring if the above holds also for other databases could lead to more statistically relevant and generalizable results as well. The bottom line of this discussion is that we suggest using some caution when a testing dataset is not available and R^2_{pred} is used as the only performance parameter. These considerations are mostly on the formal side, as all three models have a very high predictive power, which could be enough for practical purposes.

References

[1] Guruprasad Alva, Yaxue Lin, Guiyin Fang, An overview of thermal energy storage systems, Energy 144 (0360–5442) (2018) 341–378.

[2] Ibrahim Dincer, Marc A. Rosen, Thermal Energy Storage: Systems and Applications, John Wiley & Sons, 2021.

[3] D.N. Nkwetta, F. Haghighat, Thermal energy storage with phase change material—a state-of-the-art review, Sustain. Cities Soc. 10 (2014) 87–100.

[4] S. Wu, T. Yan, Z. Kuai, W. Pan, Thermal conductivity enhancement on phase change materials for thermal energy storage: a review, Energy Storage Mater. 25 (2020) 251–295.

[5] N. Tay, M. Belusko, F. Bruno, An effectiveness-NTU technique for characterizing tube-in-tank phase change thermal energy storage systems, Appl. Energy 91 (1) (2012) 309–319.

[6] N. Stathopoulos, M. El Mankibi, R. Issoglio, P. Michel, F. Haghighat, Air–PCM heat exchanger for peak load management: experimental and simulation, Sol. Energy 132 (2016) 453–466.

[7] X. Xiao, P. Zhang, M. Li, Preparation and thermal characterization of paraffin/metal foam composite phase change material, Appl. Energy 112 (0306–2619) (2013) 1357–1366.

[8] Rami M. Saeed, J.P. Schlegel, R. Sawafta, V. Kalra, Plate type heat exchanger for thermal energy storage and load shifting using phase change material, Energy Convers. Manag. 181 (0196–8904) (2019) 120–132.

[9] Wenzhu Lin, Wenbo Zhang, Ziye Ling, Xiaoming Fang, Zhengguo Zhang, Experimental study of the thermal performance of a novel plate type heat exchanger with phase change material, Appl. Therm. Eng. 178 (1359–4311) (2020) 115630.

[11] B. Gürel, A numerical investigation of the melting heat transfer characteristics of phase change materials in different plate heat exchanger (latent heat thermal energy storage) systems, Int. J. Heat Mass Transf. 148 (0017–9310) (2020) 119117.

[12] Arun K. Raj, M. Srinivas, S. Jayaraj, Transient CFD analysis of macro-encapsulated latent heat thermal energy storage containers incorporated within solar air heater, Int. J. Heat Mass Transf. 156 (0017–9310) (2020) 119896.

[13] Barış Gürel, Volkan Ramazan Akkaya, Merve Göltaş, Çağla Nur Şen, Onur Vahip Güler, Mehmet İlkay Koşar, Ali Keçebaş, Investigation on flow and heat transfer of compact brazed plate heat exchanger with lung pattern, Appl. Therm. Eng. 175 (1359–4311) (2020) 115309.

[14] Mehrdad Taghavi, Minna Poikelispää, Vaibhav Agrawal, Seppo Syrjälä, Tero Joronen, Numerical investigation of a plate heat exchanger thermal energy storage system with phase change material, J. Energy Storage 61 (2352–152X) (2023) 106785.

[15] T. Kumirai, J. Dirker, J. Meyer, Experimental analysis for thermal storage performance of three types of plate encapsulated phase change materials in air heat exchangers for ventilation applications, J. Build. Eng. 22 (2353–7102) (2019) 75–89.

[16] P. Larrinaga, G. Diarce, A. Campos-Celador, A. Garcia-Romero, Parametric characterization of a full-scale plate-based latent heat thermal energy storage system, Appl. Therm. Eng. 178 (2020) 115441.

[17] Wenye Lin, Zhenjun Ma, Haoshan Ren, Stefan Gschwander, Shugang Wang, Multi-objective optimisation of thermal energy storage using phase change materials for solar air systems, Renew. Energy 130 (0960–1481) (2019) 1116–1129.

[18] Yu-Bing Tao, Ming-Jia Li, Ya-Ling He, Wen-Quan Tao, Effects of parameters on performance of high temperature molten salt latent heat storage unit, Appl. Therm. Eng. 72 (1) (2014) 48–55.

[19] Xiaoqin Sun, Yajing Mo, Jie Li, Youhong Chu, Lihui Liu, Shuguang Liao, Study on the energy charging process of a plate-type latent heat thermal energy storage unit and optimization using Taguchi method, Appl. Therm. Eng. 164 (1359–4311) (2020) 114528.

[20] Torbjörn Lundstedt, Elisabeth Seifert, Lisbeth Abramo, Bernt Thelin, Åsa Nyström, Jarle Pettersen, Rolf Bergman, Experimental design and optimization, Chemom. Intell. Lab. Syst. 42 (0169–7439) (1998) 3–40.

[21] Kai-Tai Fang, Dennis K.J. Lin, Uniform experimental designs and their applications in industry, in: Handbook of Statistics vol. 22, Elsevier, 2003, pp. 131–170.

[22] J.L. Rosa, A. Robin, M.B. Silva, C.A. Baldan, M.P. Peres, Electrodeposition of copper on titanium wires: Taguchi experimental design approach, J. Mater. Process. Technol. 209 (3) (2009) 1181–1188.

[23] Phillip J. Ross, Taguchi Techniques for Quality Engineering: Loss Function, Orthogonal Experiments, Parameter and Tolerance Design, 1988.

[24] André I. Khuri, Siuli Mukhopadhyay, Response surface methodology, WIREs Comput. Stat. 2 (2010) 128–149.

[25] Yie Hua Tan, Mohammad Omar Abdullah, Cirilo Nolasco-Hipolito, Nur Syuhada, Ahmad Zauzi, Application of RSM and Taguchi methods for optimizing the transesterification of waste cooking oil catalyzed by solid ostrich and chicken-eggshell derived CaO, Renew. Energy 114 (0960–1481) (2017) 437–447.

[26] Xinyu Huang, Fangfei Li, Yuanji Li, Xiangzhao Meng, Xiaohu Yang, Bengt Sundén, Optimization of melting performance of a heat storage tank under rotation conditions: based on taguchi design and response surface method, Energy 271 (0360–5442) (2023) 127100.

[27] Xinyu Huang, Fangfei Li, Tian Xiao, Yuanji Li, Xiaohu Yang, Ya-Ling He, Structural optimization of melting process of a latent heat energy storage unit and application of flip mechanism, Energy 280 (0360–5442) (2023) 128164.

[28] K.R. Milkey, A.R. Samsudin, A.K. Dubey, P. Kidd, et al., Comparison between Taguchi method and Response Surface Methodology (RSM) in modelling CO2 laser machining, Jordan J. Mech. Ind. Eng. 8 (2014).

[29] Hossein Soltani, Madjid Soltani, Hassan Karimi, Jatin Nathwani, Optimization of shell and tube thermal energy storage unit based on the effects of adding fins, nanoparticles and rotational mechanism, J. Clean. Prod. 331 (0959–6526) (2022) 129922.

[30] S. Minetto, Theoretical and experimental analysis of a CO2 heat pump for domestic hot water, Int. J. Refrig. 34 (0140–7007) (2011) 742–751.

[31] Giti Nouri, Younes Noorollahi, Hossein Yousefi, Designing and optimization of solar assisted ground source heat pump system to supply heating, cooling and hot water demands, Geothermics 82 (0375–6505) (2019) 212–231.

[32] A.K. Raj, M. Srinivas, S. Jayaraj, 156:119896. Available from: transient CFD analysis of macro-encapsulated latent heat thermal energy storage containers incorporated within solar air heater, Int. J. Heat Mass Transf. 156 (2020) 119896.

[33] Mithat Akgün, Orhan Aydın, Kamil Kaygusuz, Experimental study on melting/solidification characteristics of a paraffin as PCM, Energy Convers. Manag. 48 (0196–8904) (2007) 669–678.

[34] Russell Lenth, Response-surface methods in R, using rsm, J. Stat. Softw. 32 (2010).

[35] G.E.P. Box, D.W. Behnken, Some new three level designs for the study of quantitative variables, Technometrics 2 (1960) 455–475.

[36] Long Gao, Gegentana, Zhongze Liu, Baizhong Sun, Deyong Che, Shaohua Li, Multi-objective optimization of thermal performance of packed bed latent heat thermal storage system based on response surface method, Renew. Energy 153 (2020) 669–680.

[37] C. Liu, H. Yang, Multi-objective optimization of a concrete thermal energy storage system based on response surface methodology, Appl. Therm. Eng. 202 (2022) 117847.

[39] C.G. Atkeson, A.W. Moore, S. Schaal, Locally weighted learning, Artif. Intell. Rev. 11 (February 1997) (1997) 11–73.

[40] K. Deb, A. Pratap, S. Agarwal, T. Meyarivan, A fast and elitist multiobjective genetic algorithm: NSGA-II, IEEE Trans. Evol. Comput. 6 (2002) 182–197.

[41] Maureen C. Kennedy, E. David Ford, Peter Singleton, Mark Finney, James K. Agee, Informed multi-objective decision-making in environmental management using Pareto optimality, J. Appl. Ecol. 45 (2008) 181–192.

[42] Nemanja Koruga, Mirko Dobrnjac, Dušan Golubović, Nemanja Dobrnjac, Analysis of the influence of condensation temperature and compressor efficiency on heat pump system efficiency, in: IOP Conference Series: Materials Science and Engineering, 2021.

[43] Ali Jahan, Kevin Edwards, Multi-Criteria Decision Analysis for Supporting the Selection of Engineering Materials in Product Design, 2013.